Applied Catalysis B: Environmental 140–141 (2013) 468–477

Contents lists available at SciVerse ScienceDirect

Applied Catalysis B: Environmental

journal homepage: www.elsevier.com/locate/apcatb

# Degrading perchloroethene at ambient conditions using Pd and Pd-on-Au reduction catalysts

Zhun Zhao[a], Yu-Lun Fang[a], Pedro J.J. Alvarez[b], Michael S. Wong[a,b,c,*]

[a] Department of Chemical and Biomolecular Engineering, Houston, TX 77005, United States
[b] Department of Civil and Environmental Engineering, Houston, TX 77005, United States
[c] Department of Chemistry, Rice University, 6100 Main Street, Houston, TX 77005, United States

ARTICLE INFO

*Article history:*
Received 10 October 2012
Received in revised form 28 February 2013
Accepted 12 April 2013
Available online xxx

*Keywords:*
Tetrachloroethene
Perchloroethene
Palladium
Gold
Hydrodechlorination
Nanoparticles

ABSTRACT

Perchloroethene (PCE) is a common groundwater contaminant, due to its common use as a dry-cleaning solvent. Current treatment methods are limited in their ability to remove PCE from contaminated sites in an efficient and cost effective manner. Palladium-on-gold nanoparticles (Pd-on-Au NPs) have been shown to be highly catalytically active in the hydrodechlorination (HDC) of trichloroethene (TCE) and other chlorinated compounds. However, the catalytic chemistry of such nanoparticles for PCE HDC in water has not been systematically addressed in the literature. In this paper, we assess the catalytic properties of ~4 nm Pd-on-Au NPs, ~4 nm Pd NPs, and $Pd/Al_2O_3$ for water-phase PCE HDC under ambient conditions. The Pd-on-Au NPs exhibited volcano-shape activity as a function of Pd surface coverage (sc). Maximum activity was at 80 ± 0.8 sc% (pseudo-first order rate constant of ~5000 $L/g_{Pd}$/min), which was ~20× and ~80× higher than that for Pd NPs and $Pd/Al_2O_3$ at room temperature and pH 7. A complete mechanistic model of PCE HDC that coupled gas–liquid mass transfer with the surface reactions was developed and found to be consistent with the observed concentration-time profiles for the 3 catalyst types. The formation and subsequent reaction of daughter products (TCE, dichloroethene isomers, vinyl chloride, and ethene) followed the stepwise dechlorination of the PCE chlorine groups. The final reaction products were ethane and minor amounts of n-butane/butenes. This study establishes the enhanced degradation chemistry of PCE using model Pd-on-Au catalysts and suggests the volcano-shape structure-activity dependence can be generalized from PCE and TCE to other organohalides.



## 1. Introduction

In urban or heavily populated areas, the extensive use of perchloroethene (PCE, "perc", or tetrachloroethene) as the predominant dry cleaning solvent since 1935 has led to its widespread contamination at an estimated 27,000 sites (75% of all dry cleaning facilities) in the U.S., impacting a significant number of private and public water supply wells while threatening many other well areas [1,2]. PCE is a known central nervous system depressant and is classified by the U.S. Environmental Protection Agency (U.S. EPA) to be a likely human carcinogen [3]. Alternative solvents are being phased in [4,5], but PCE is still used in 75% of the professional cleaners in the U.S. [6].

PCE, mixed with other chlorocarbons like trichloroethene (TCE) and trichloroethane, is also used as a metal degreaser at electronic manufacturing plants and military facilities (many of which are deemed National Priority List Superfund sites) [7,8]. It is found in at least 771 of the 1430 Superfund sites above its maximum contaminant level (MCL) of 5 μg/L (=5 ppb = 30 nM) in drinking water [9,10]. PCE was also identified by European Environment Agency (EEA) as one of the most frequently detected volatile organic compounds in groundwater aquifers of most Western European countries [11–13]. In China, PCE pollution has been widely regarded as a serious problem in the delta region of rivers (Yangtze, Pearl, etc.) and in 2005 a northern city in China even reported a PCE concentration of 488 ppb in shallow groundwater, almost two orders of magnitude higher than U.S. EPA MCL [14,15].

Upon its release into the environment, PCE, having a density greater than that of water (1.62 g/mL), can accumulate into dense non-aqueous phase liquid (DNAPL) pools beneath the water table and slowly dissolve (up to the solubility limit of PCE in water at 20 °C of 150 mg/L = 0.91 mM) to form large plumes that persist over long periods of time. Untreated PCE (ranked as 33rd most toxic, prevalent, and accessible substance at Superfund sites [10]) is a problem because natural biotic degradation can transform it into even more harmful substances such as TCE (ranked 16th) and vinyl chloride (VC, ranked 4th) [2,10,16,17].

* Corresponding author at: Department of Chemical and Biomolecular Engineering, Rice University, Houston, TX 77005, United States. Tel.: +1 713 348 3511; fax: +1 713 348 5478.
*E-mail address:* mswong@rice.edu (M.S. Wong).

0926-3373/$ – see front matter © 2013 Elsevier B.V. All rights reserved.
http://dx.doi.org/10.1016/j.apcatb.2013.04.032

**Nomenclature**

| | |
|---|---|
| $a_{gl}$, $a_s$ | specific areas for gas–liquid interface and NP catalyst solid surface in overall batch reactor liquid volume |
| $a_{s-ex}$, $a_i$ | specific areas for external and internal surface for $Pd/Al_2O_3$ in overall batch reactor liquid volume |
| $k_{gl}$, $k_{ls}$, $k_i$ | mass transfer coefficients for gas–liquid, liquid–solid, and intraparticle processes |
| $k$, $k_{meas}$ | rate constant for overall surface reaction, and observed rate constant for overall reaction |
| $k_{cat}$, $k_{cat'}$, $k_{cat,corr}$ | apparent rate constant normalized with total Pd content, rate constant normalized with surface Pd content and mass transfer-corrected rate constant |
| $C_{Pd}$, $C_{Pd'}$ | Pd metal content and surface Pd metal content in the reactor |
| $C_{PCE}$, $C_{PCE,0}$ | PCE liquid-phase concentration and initial PCE liquid-phase concentration |
| $C_1$, $C_2$ | $Y$-intercept and slope of $1/k_{meas} - 1/C_{Pd}$ plot |
| $k_{PCE}$, $k_{TCE}$, $k_{DCEi}$, $k_{VC}$, $k_{ethene1}$, $k_{ethene2}$, $k_{butene}$ | surface reaction rate constants for elementary reaction step from PCE to TCE, from TCE to one DCE isomer, from one DCE isomer to VC, from VC to ethene, from ethene to ethane, from ethene to butene, and from butene to butane |
| $K$ with subscript | surface adsorption–desorption equilibrium constant for a given compound |
| [PCE] | liquid phase concentration for PCE |
| $[S]_{total}$ | total concentration of active sites |

Methods of managing PCE contaminated groundwater are similar to those of TCE, which include hydraulic control of the plume (to mitigate migration) using *ex situ* pump-and-treat technologies of air stripping and activated carbon adsorption [18–20]. These physico-chemical methods are imperfect, though, as they only transfer the contaminants from one phase to another and do not destroy them.

Another approach involves *in situ* treatment of PCE, in which the contaminant is broken down chemically in the subsurface, such as reactive remediation [21–23], thermal treatment [24], and bioremediation [25,26]. With reactive remediation, PCE can be degraded through either oxidative or reductive means. Oxidative remediation involves injecting a large quantity of an oxidant such as potassium permanganate [22,27], into known contaminated areas. Reductive remediation involves the use of a reductant, with the most widely used material being zero-valent iron (ZVI). In granular or powder form, ZVI is commercially available for remediation applications [28–32] and commonly deployed in permeable reactive barriers (PRBs) [33–36]. A newer development is the use of nanoparticulate zero valent iron (NZVI) to penetrate PCE contamination zones after subsurface injection [37–40].

The use of palladium (Pd) catalysts has been well studied for the reductive remediation of TCE and other chlorinated ethenes in water [41–47]. This technique is advantageous over others as palladium converts the chlorinated ethenes *via* hydrodechlorination (HDC) to non-toxic ethane with high reaction rates and with minimal formation of chlorinated side products. Our group has shown that palladium-coated gold nanoparticles (Pd-on-Au NPs) have much higher TCE HDC catalytic activity and greater resistance to chloride and sulfide deactivation compared to $Pd/Al_2O_3$ and Pd NPs [45–50]. Comparison of field-test results of different TCE treatment technologies indicated that the cost of treating the same volume of TCE-contaminated water using Pd catalysis was comparable to that of air-stripping and less expensive than granulated carbon adsorption and permeable reactive barrier [51].

Beyond our early observation of Pd-on-Au NPs showing high activity for PCE HDC [47], there are few reports on Pd-based catalysts for PCE degradation in water under ambient conditions. Some reports on Pd catalysts for PCE degradation described results for high-temperature gas-phase conditions [52–54] and for non-aqueous media under ambient conditions [55–57]. Other work discussed the use of Pd-doped NZVI in the *in situ* destruction of PCE under ambient conditions, in which Pd was the catalyst and iron was the reducing agent [58–61]. In this work, we studied Pd-on-Au NPs for PCE HDC in water using $H_2$, at room temperature, and at atmospheric pressure. We quantified the catalytic activities of $Pd/Al_2O_3$, Pd NPs, and Pd-on-Au NPs, and tested the hypothesis that the NPs exhibited volcano-shape activity dependence for PCE HDC due to the molecular similarity of PCE and TCE.

## 2. Materials and methods

### 2.1. Synthesis

Briefly, Au NPs (~4 nm) were synthesized *via* a sodium citrate reduction [46,62]. Pd-on-Au NPs with Pd surface coverages of 10, 20, 40, 50, 60, 67, 80, 90, 100, 150 and 300 sc% were prepared by reducing specified volumes of a $H_2PdCl_4$ solution onto Au NPs by $H_2$ gas. Pd NPs (~4 nm) were synthesized using a similar procedure for Au NP synthesis. The synthesis details are found in Supplementary Information. A supported Pd catalyst in the form of $Pd/Al_2O_3$ (Sigma–Aldrich, 1 wt% Pd, average particle size 38–70 μm [43], specific surface area 177 $m^2/g$ [45], pore volume 0.20 $cm^3/g$ [43]) was also tested as received.

### 2.2. Characterization

The synthesized NPs were imaged using a JEOL 2010 transmission electron microscope (TEM). TEM samples were prepared by depositing NP sol onto a 200-mesh carbon/Formvar TEM grid which was then dried under room temperature. The ImageJ program was used for the size distribution measurements [63]; 250 particles were measured for each sample. Other characterization results can be found in our previous studies [46,50].

### 2.3. Reaction testing

The batch reactor was prepared by adding 30 mL of a citrate buffer solution to ~140–143 mL of DI water in a 250 mL serum bottle, such that the resulting pH was 7.0. The citrate buffer solution was prepared by dissolving 2.58 g of trisodium citrate (>99.5%, Fisher) into 100 mL DI water and then adjusting the pH to 7.0 using 0.1 M citric acid (prepared separately by dissolving 0.21 g of citric acid (>99.5%, Fisher) into 100 mL of DI water). The bottle was sealed with Teflon tape and a Teflon-coated rubber septum. Hydrogen gas was bubbled through the water for 15 min, filling the headspace. 3 μL of PCE (99.5%, Sigma–Aldrich) and 0.2 μL of pentane (99.7%, Burdick and Jackson) were injected into the reactor as the reactant and internal standard, respectively. The contents were stirred vigorously for 3 h, sufficient for the sealed batch reactor to reach equilibrium.

Pd-on-Au NP sols (with varying Pd surface coverages) were then charged to the batch reactor, such that the total amount of Pd metal (6.81 μg of Pd metal) was the same. For the Pd-on-Au NP with 0 sc% sample, 1 mL of Au NP sol was used. For Pd NPs and $Pd/Al_2O_3$, 1 mL of Pd NP sol and 1 mL of $Pd/Al_2O_3$ powder suspension (25 mg/mL) were charged, respectively, corresponding to 31.8 and 250 μg of Pd metal charged. The total liquid amount was set to be 173 mL. The PCE HDC reaction was carried out at room temperature (23 ± 1 °C)

under constant magnetic stirring (800 rpm). Each experiment was performed at least twice. The conversion results were averaged and were within ±15%. Headspace gas chromatography was used to monitor the reaction, with catalyst injection marking the start of the reaction (Supplementary Information).

### 2.4. Reaction data analysis

GC peaks corresponding to PCE, TCE, ethane, 1,1-DCE, *cis*-1,2-DCE, *trans*-1,2-DCE, VC, ethene, *n*-butane, and butenes (mixture of isomers) were quantified as gas-phase concentrations in headspace of the reactor. Gas-phase and liquid-phase concentrations were calculated from the total moles of each species injected using Henry's law and the appropriate dimensionless Henry's law constants $H_{cc}$ (= aqueous concentration/gas concentration) for PCE, TCE, ethane, 1,1-DCE, *cis*-1,2-DCE, *trans*-1,2-DCE, VC, ethene, *n*-butane and butenes (0.641, 0.339, 0.0485, 0.999, 0.145, 0.352, 0.999, 0.114, 0.0267, and 0.0340 at 23 °C, respectively) [64–67]. For example, 3 μL of PCE in the 250 mL serum bottle containing 173 mL liquid gives a total mole of 29.3 μmol, a gas-phase concentration of 0.156 mM and a liquid-phase concentration of 0.100 mM (=16.6 ppm) in the reactor after equilibration. The carbon balance was defined as the total number of carbons of the remaining PCE, products and by-products in the batch reactor, divided by the total number of carbons of the initial PCE amount.

PCE HDC activity was reported for all catalysts assuming first-order reaction kinetics. Reaction rate constants were calculated using $C_{PCE} = C_{PCE,0} \times \exp(-k_{meas}t)$ with $C_{PCE,0}$ is initial PCE liquid-phase concentration, $k_{meas} = k_{cat} \times C_{Pd}$, $k_{cat}$ is the first-order, Pd-normalized rate constant (with units of L/$g_{Pd}$/min), $C_{Pd}$ is the Pd content in the reactor, and $t$ is reaction time. For a given catalyst composition, the rate constant $k_{cat}$ was the average value of three runs ± 1 standard deviation. Another rate constant $k_{cat'}$ (with units of L/$g_{surfacePd}$/min) that accounted for surface Pd atom content was calculated from $k_{meas} = k_{cat'} \times C_{Pd'}$, where $C_{Pd'}$ is the surface Pd content in the reactor. For Pd surface coverages less than 100 sc%, all Pd atoms were assumed to be surface Pd atoms. For Pd surface coverages greater than 100 sc%, the surface Pd content was calculated assuming a magic cluster model of the Pd-on-Au NPs [46,68–70]. For example, the surface atoms of 150 sc% Pd-on-Au NPs were counted as those Pd atoms in the 9th shell and those Pd atoms in 8th shell that were not covered. Pd dispersion (percentage of Pd atoms as surface atoms) for Pd NPs was calculated to be 25% from the empirically derived relation: dispersion = $c/d$, where $c$ is a constant 1.1 for Pd, and $d$ is the average particle size (4.4 nm from TEM) [50,71,72]. The dispersion for $Pd/Al_2O_3$ was 21% [43,48]. PCE conversion was calculated as $(C_{PCE,0}-C_{PCE})/C_{PCE,0}$. We verified that the $k_{cat}$ did not vary at different catalyst charges for the experimental conditions used, which can occur when too much catalyst is used.

## 3. Results and discussion

### 3.1. Confirmation of NP sizes

Typical TEM images for Au NPs, 80 sc% Pd-on-Au NPs, and Pd NPs are shown in Fig. 1. The mean diameters (and relative standard deviations) were measured to be 4.1 nm (21%), 4.2 nm (22%), and 4.4 nm (32%) for Au NPs, 80 sc% Pd-on-Au NPs, and Pd NPs, respectively, consistent with our previous studies [46–48,50].

### 3.2. Assessing mass transfer effect on rate constants

Various amounts of 60 sc% Pd-on-Au NP sol were injected into the batch reactor and the rate constant $k_{meas}$ values were recorded. Specifically, 0, 0.233, 0.467, 0.933 and 1.866 mL of sol were charged, such that the corresponding Pd content of the reactor was 0, $0.985 \times 10^{-5}$, $1.97 \times 10^{-5}$, $3.94 \times 10^{-5}$, and $7.88 \times 10^{-5}$ $g_{Pd}$/L. The $k_{meas}$ values varied linearly with $C_{Pd}$ from 0 to $3.94 \times 10^{-5}$ $g_{Pd}$/L, with the slope equal to a $k_{cat}$ value of 2413 L/$g_{Pd}$/min (Fig. S1a). This was within 10% of the $k_{cat}$ value determined for 60 sc% Pd-on-Au NPs using the standard catalyst charge of $3.94 \times 10^{-5}$ $g_{Pd}$/L (2406 L/$g_{Pd}$/min, Table S1). That the standard catalyst charge was in this linear regime indicated the $k_{cat}$ values determined for all other catalytic materials were independent of catalyst amount.

The mass transfer resistances were determined in a manner developed previously for the TCE HDC reaction [49]. Plotting the reciprocal of the non-zero $k_{meas}$ and $C_{Pd}$ values allowed the gas–liquid and liquid-catalyst surface resistances ($1/k_{gl}a_{lg}$ and $1/k_{ls}a_s$) and surface reaction rate contribution ($1/ka_s$) to be determined using the relation $1/k_{meas} = C_1 + C_2 \times 1/C_{Pd}$ (Fig. S1b). The $y$-intercept $C_1$ related to $1/k_{gl}a_{gl}$ and the slope $C_2$ related to $1/k_{ls}a_s$ and $1/ka_s$, where $k_{gl}$ is the gas–liquid mass transfer coefficient, $a_{gl}$ is the gas–liquid interface specific areas, $k_{ls}$ is the liquid–solid mass transfer coefficient, $a_s$ is the particle specific surface areas, and $k$ is the rate constant for surface reaction. The value of $1/k_{ls}a_s$ term was calculated to be 0.00853 min based on the diffusivity of PCE ($8.2 \times 10^{-6}$ $cm^2$ $s^{-1}$ at 25 °C [73]). The $1/k_{gl}a_{lg}$, $1/k_{ls}a_s$ and $1/ka_s$ terms were then determined to be 0.473, 0.00853 and 10.1 min, respectively. Comparison of their values (i.e., $1/ka_s > 1/k_{gl}a_{lg} \gg 1/k_{ls}a_s$) indicated that the liquid-solid mass transfer was the most rapid among the three processes, and the gas–liquid mass transfer was slow enough to affect observed reaction rate constants. To exclude the gas–liquid mass transfer effect, $k_{cat}$ should be re-calculated as $k_{cat,corr}$ using the relation $k_{cat,corr} = ka_s/C_{Pd}$. However, the gas–liquid mass transfer effect was deemed to be small, based on the calculated $k_{cat,corr}$ (2512 L/$g_{Pd}$/min) being only 4% higher than $k_{cat}$ (2406 L/$g_{Pd}$/min, Table S1). Only for the most active catalyst (80 sc% Pd-on-Au NPs) was the calculated $k_{cat,corr}$ (5477 L/$g_{Pd}$/min) 10% higher than $k_{cat}$ (4971 L/$g_{Pd}$/min, Table S1). Thus, $k_{cat,corr}$ values were not calculated for the rest of the catalyst compositions in this study. An analogous experimental mass transfer analysis of the $Pd/Al_2O_3$ comparison sample was not carried out. The major structural differences between $Pd/Al_2O_3$ and the NPs were the larger particle size and the internal pores of the former, leading to a different liquid–solid mass transfer resistance and a possible intraparticle diffusional effect. The liquid–solid mass transfer resistance was estimated with an earlier method of ours [46] and the intraparticle mass transfer effect was determined from the Thiele modulus and effectiveness factor. Our calculations indicated the liquid–solid mass transfer resistance was small and internal diffusion was a negligible effect (Supplementary Information).

### 3.3. Catalytic activity

Pd-on-Au NPs with Pd surface coverages ranging from 0 to 300 sc%, Pd NPs, and supported Pd catalysts were tested for PCE HDC reaction ($Cl_2C=CCl_2 + 5H_2 \rightarrow H_3C-CH_3 + 4HCl$). All materials were active for the reaction, except for control Pd-on-Au NPs with 0 sc%, i.e., Au-only NPs (Fig. 2, Table S1). The total Pd content in the batch reactor was kept the same for Pd-on-Au NPs regardless of Pd surface coverage, and so the differences in rate constants were clearly due to the different states of Pd metal on the Au surface. PCE conversion increased with increasing Pd surface coverage, up to 80 sc% (Fig. 2a). The PCE conversion decreased for NPs with surface coverages that exceeded 80 sc%, to the point where Pd-on-Au NPs with 300 sc% (which had 42.4 wt% Pd of total metal content) was less active than Pd-on-Au NPs with 20 sc% (which had 4.7 wt% Pd of metal content) (Fig. 2b). The 80 sc% Pd-on-Au NP sample was more active than Pd NPs (which contained ~5× more Pd) and $Pd/Al_2O_3$ (which contained ~37× more Pd) (Fig. 2c). While the conversion-time

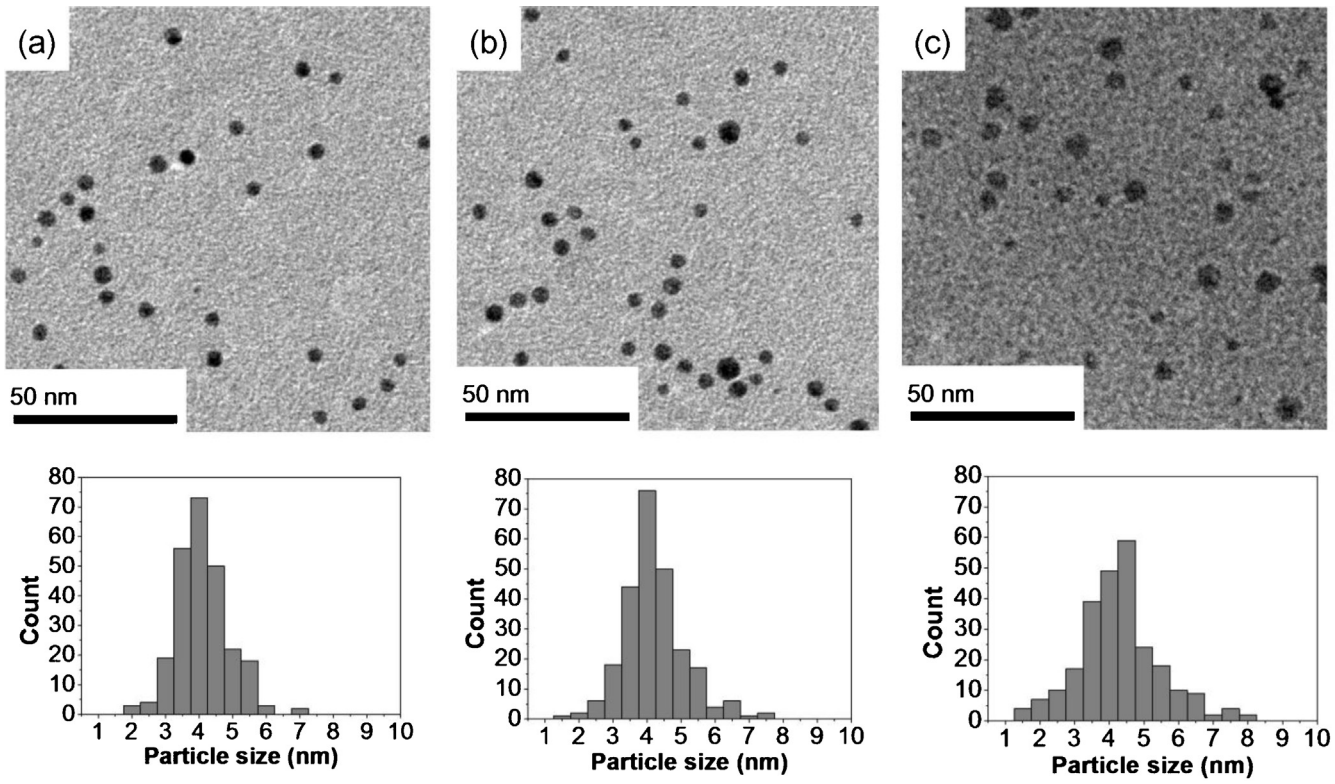


**Fig. 1.** TEM images and corresponding particle size histograms of (a) Au NPs, (b) 80 sc% Pd-on-Au NPs, and (c) Pd NPs. Each bar represents the total number of NPs of a particle diameter ±0.25 nm.

profiles for some samples did not have a clear exponential time dependence, the assumption of first-order kinetics was sufficient to show clear activity trends with Pd surface coverage.

The Pd-on-Au NPs had a volcano-shape dependence on surface coverage, with the maximum activity corresponding to 80 sc% (Fig. 2d). They were much more active than Pd NPs and $Pd/Al_2O_3$ on a per-gram Pd basis (238 and 60 $L/g_{Pd}/min$). Accounting for only surface Pd atoms, the reaction rate constants for samples with >100 sc% had comparable values (~2600–2633 $L/g_{surfacePd}/min$). Presumably overcoated with Pd metal, these NPs were several times more active than Pd NPs and $Pd/Al_2O_3$, which had corresponding rate constants of 952 and 167 $L/g_{surfacePd}/min$. This difference in catalytic activity may be the result of Au electronic effects imposed upon the outermost Pd atoms [46]. Such electronic promotional effects have been observed in many other reaction systems involving bimetallic PdAu catalysts or electrodes, such as cyclization of acetylene to benzene [74], electrochemical oxidation of formic acid [75] and benzyl alcohol oxidation [76] and substantiated by DFT (density functional theory) calculations [77,78].

The volcano-shape feature for the PCE HDC reaction was similar to that for TCE HDC, suggesting a similar dependence on the Pd-on-Au catalyst nanostructure. In our structural model of Pd-on-Au NPs developed for the latter reaction [50,79], the Pd is in the form of isolated atoms and few small two-dimensional ensembles at the lowest surface coverages, correlating to the lower catalytic activity per-Pd-atom. The per-Pd-atom catalytic activity increases at higher surface coverages, indicative of more active two-dimensional Pd ensembles; it decreases beyond ~60–70 sc%, which is now attributed to the emergence of less active, three-dimensional Pd ensembles [79].

A notable difference was the PCE HDC volcano peak being located at a higher surface coverage (~80 sc%) than the ~60–70 sc% peak for TCE HDC. This difference was statistically real because the 80 sc% value had an uncertainty of 0.8 sc% (one standard deviation based on error propagation analysis, Supplementary Information) and the 70 sc% value has an uncertainty of 2.6 sc% (one standard deviation based on inductively coupled plasma-optical emission spectroscopy results of 70 sc% 3 nm Pd-on-Au NPs from a previous study [79]). The structure for Pd-on-Au NPs at any Pd surface coverage is the same for either reaction, and so this peak offset indicated the active site that gave the highest activity for PCE HDC differed slightly from the active site that gave the highest activity for TCE HDC.

To provide a sense of the materials costs of the most active Pd-on-Au NP catalyst and Pd NPs, we calculated the amount of Pd and Au needed to degrade PCE (dissolved in water) from 100 ppm to 5 ppb for the same reaction time (Table S2). With January 2013 spot prices of palladium (~710 US$/oz) and gold (~1670 US$/oz), Pd-on-Au NPs were ~1.6× less expensive than Pd NPs. A practical water treatment technology requires flow conditions, and so a supported version of the bimetallic would be needed. We performed a similar cost analysis using flow performance results for the TCE HDC reaction in comparing the cost of ion-exchange resin supported Pd-on-Au NPs and commercial $Pd/Al_2O_3$, and we concluded that the former material cost ~18× times less than the latter [47]. Further refinement of the cost analysis requires additional information about catalyst performance in field tests (accounting for mass transfer effects, deactivation resistance, and regenerability), capital costs, and operational costs.

### 3.4. Selectivity differences

The products formed from PCE HDC were plotted with time for 60 sc% Pd-on-Au NP, Pd NP, and $Pd/Al_2O_3$ samples (Fig. 3). Much more Pd metal was charged for the $Pd/Al_2O_3$ case (Table S1), resulting in the faster PCE conversion compared to the other two cases. Carbon balance at all time points for the three catalysts was 100 ± 5%.

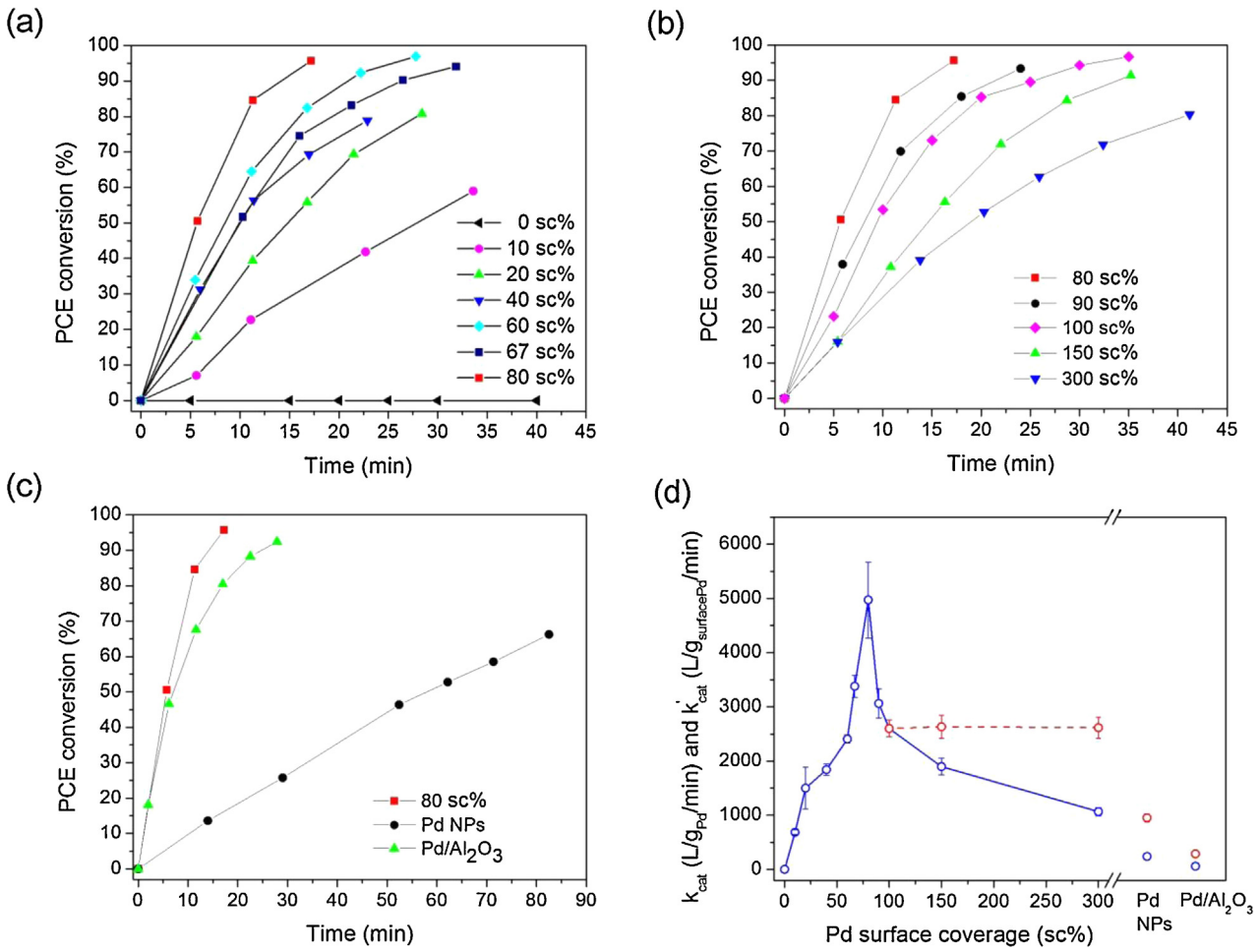


**Fig. 2.** PCE conversion profiles for Pd-on-Au NPs with (a) 0–80 sc%, (b) 80–300 sc%, and for (c) Pd NPs and $Pd/Al_2O_3$ catalysts. (d) PCE HDC $k_{cat}$ (blue) and $k_{cat}$' (red) values plotted (with error bars of ±1 standard deviation) against surface coverage for Pd-on-Au NPs. Reaction conditions: $C_{Pd} = 3.94 \times 10^{-5}$, $1.84 \times 10^{-4}$, and $1.45 \times 10^{-3}$ $g_{Pd}$/L for Pd-on-Au NPs, Pd NPs, and $Pd/Al_2O_3$, respectively, 23 °C, atmospheric pressure, $H_2$ headspace, pH 7.0, citrate buffer, $C_{PCE,0} = 16.6$ ppm = 0.1 mM. (For interpretation of the references to color in this figure legend, the reader is referred to the web version of the article).

PCE nearly reached full conversion in less than 1 h with Pd-on-Au NPs (Fig. 3a). At the end of the reaction, 94.6% of the product formed was ethane. Byproducts included n-butane (2.1%) and butenes (3.3%) (Fig. 3b). At intermediate reaction times, TCE, all three DCE isomers, and VC were detected, with concentrations peaking at ~5 min into the reaction. No ethene was detected at any time. These trends held true for Pd-on-Au NPs with <100 sc% and also for Pd-on-Au NPs ≥100 sc%.

PCE reached ~86% conversion after 2 h with Pd NPs (Fig. 3c). The majority of the product formed at the end of the reaction was ethane (87.5%) with n-butane (3.2%) and butenes (5.8%) also detected. TCE, all three DCE isomers, and VC were also detected at intermediate reaction times, and they existed with small amounts (3.5% in total) at the end of the reaction due to slow reaction rate of Pd NPs. The peaking times observed for these intermediate species are different for Pd NPs, with TCE and *cis*-1,2-DCE being at ~30 min, and *trans*-1,2-DCE, 1,1-DCE and VC being at ~60–70 min. Ethene was detected in trace amounts throughout the reaction.

With 36.8× more Pd charged than the 60 sc% case, PCE reached 92% conversion at 28 min with $Pd/Al_2O_3$. Ethane had a mole percentage of 99%, with the rest 1% being n-butane. At intermediate reaction times, TCE, *cis*-1,2-DCE and 1,1-DCE were the only chlorinated ethenes detected. Similar to Pd NPs, TCE and *cis*-1,2-DCE for $Pd/Al_2O_3$ peaked at approximately the same time (~2 min), while *trans*-1,2-DCE spiked at a later time (~6 min).

At intermediate PCE conversions (e.g., 40%), the distribution among the three DCE isomers interestingly differed among the 3 catalyst types (Fig. 4). The relative amounts for Pd-on-Au NPs were roughly 53% *cis*-1,2-DCE, 44% 1,1-DCE, and 3% *trans*-1,2-DCE at 40% PCE conversion, over a wide range of surface coverages. The DCE isomer distributions had a weak dependence on Pd surface coverage, with *cis*-1,2-DCE amount slightly decreased with increasing Pd surface coverage and 1,1-DCE amount slightly increased. For 300 sc% Pd-on-Au NPs, the *cis*-1,2-DCE amount (45%) was slightly smaller than the 1,1-DCE amount (53%). The selectivity to the three DCE isomers at 40% PCE conversion was 4.3% for 60 sc% Pd-on-Au NPs.

The selectivity to the DCE isomers at 40% PCE conversion for Pd NPs and $Pd/Al_2O_3$ was 7.5% and 1.5%, respectively. Compared to the Pd-on-Au NP case, relatively more *trans*-1,2-DCE (16%) and less 1,1-DCE (25%) were formed with Pd NPs. With $Pd/Al_2O_3$, cis-1,2-DCE (72%) and 1,1-DCE (28%) were formed but no *trans*-1,2-DCE was formed (Fig. 4b). As a comparison, the thermodynamic equilibrium amounts of the 3 isomers at 25 °C are 40% *cis*-1,2-DCE, 43% 1,1-DCE, and 17% *trans*-1,2-DCE (calculated from their respective standard Gibbs free energy of formation, 24.16, 24.33, and 26.54 kJ/mol [80]).

A recent DFT study by Andersin and Honkala found that the three DCE isomers had different adsorption energies on Pd-on-Au and Pd(1 1 1) surfaces [81]. *trans*-1,2-DCE was calculated to have a larger free energy of adsorption (−1.18 eV on

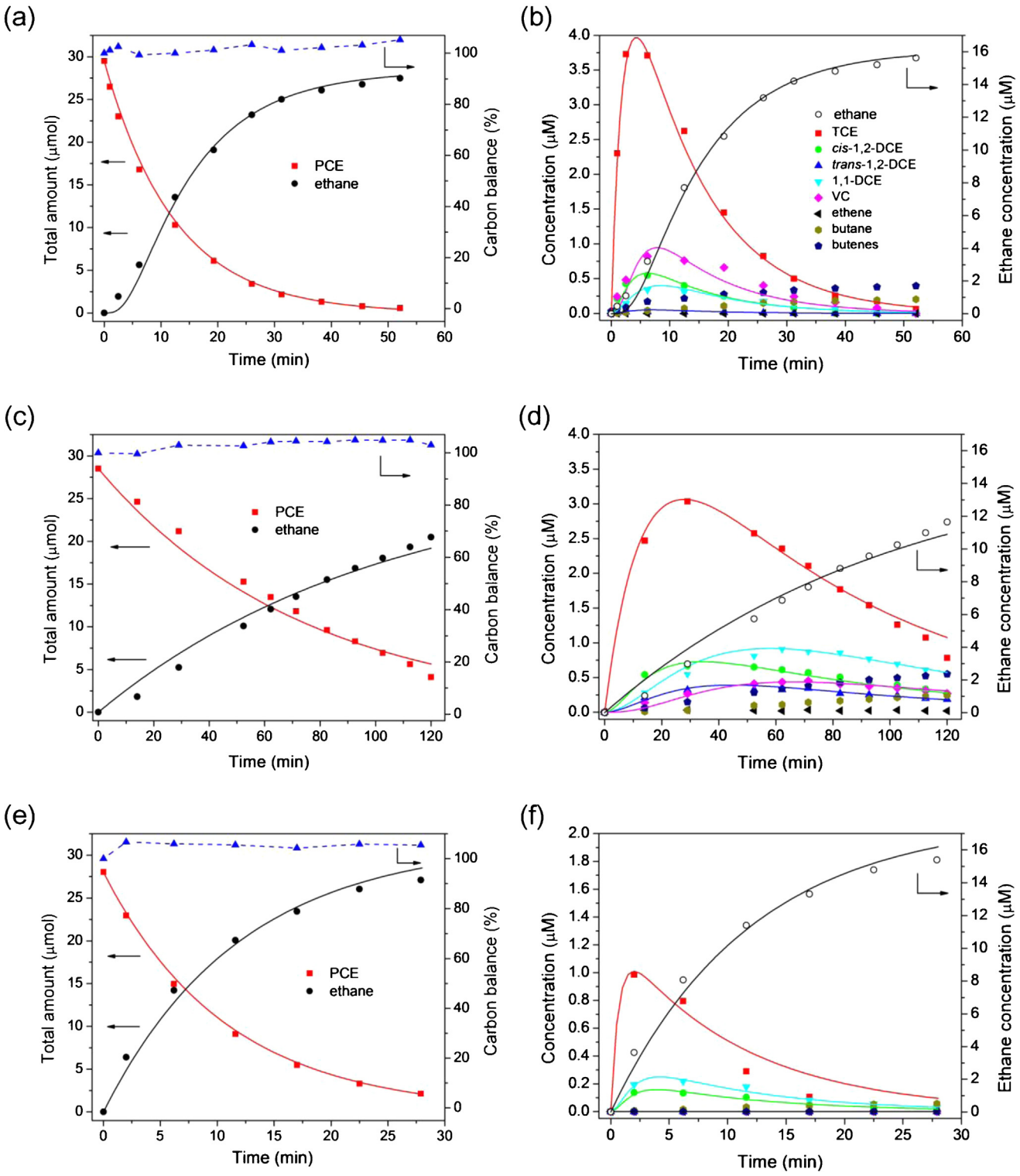


**Fig. 3.** Reaction profiles of PCE HDC using (a) 60 sc% Pd-on-Au NPs, (c) Pd NPs, and (e) $Pd/Al_2O_3$. The concentration-time profiles of reaction products during PCE HDC using (b) 60 sc% Pd-on-Au NPs, (d) Pd NPs, and (f) $Pd/Al_2O_3$. Solid lines are best-fit curves ($R^2 > 0.96$) using a modified Langmuir-Hinshelwood kinetic model (Eqs. (1)–(4), (8), and the dashed blue lines are the measured carbon balances. Reaction conditions: $C_{Pd} = 3.94 \times 10^{-5}$, $1.84 \times 10^{-4}$, and $1.45 \times 10^{-3}$ $g_{Pd}$/L for 60 sc% Pd-on-Au NPs, Pd NPs, and $Pd/Al_2O_3$, respectively, 23 °C, 1 atm, $H_2$ headspace, pH 7.0, citrate buffer, $C_{PCE,0} = 16.6$ ppm = 0.1 mM. The 60 sc% sample was chosen over the 80 sc% one due to experimental limitations (the reaction was too rapid for the GC measurements to yield smooth concentration-time profiles).

7-Pd-atom ensembles on a gold slab, $Pd_7/Au$) than either 1,1-DCE and *cis*-1,2-DCE (−1.10 eV for both). If one considers the relation between the Gibbs free energy of adsorption and adsorption equilibrium constant ($K_{ads} = \exp[-\Delta G_{ads}/kT]$), the larger the adsorption energy is, the "stickier" the adsorbed species is to the surface. Thus, *trans*-1,2-DCE adsorbs more strongly than *cis*-1,2-DCE and 1,1-DCE, resulting in its lower solution-phase concentration (consistent with the experimental data). Also contributing to this lower concentration is the higher reactivity of *trans*-1,2-DCE for HDC (2303 L/$g_{Pd}$/min), compared to *cis*-1,2-DCE (1813 L/$g_{Pd}$/min) and

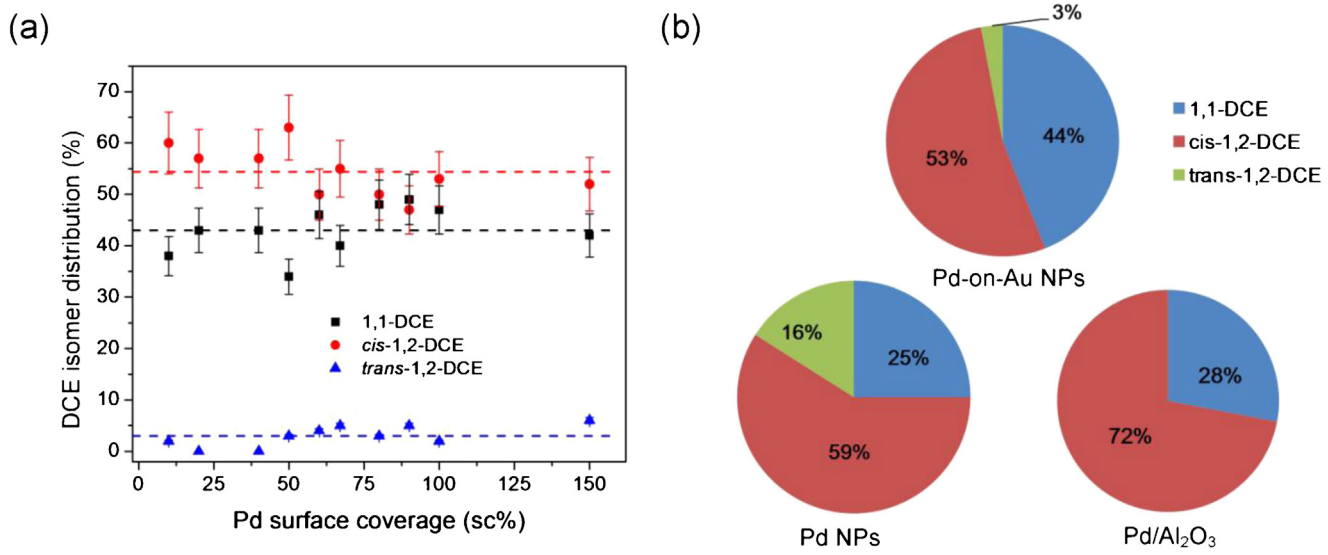


**Fig. 4.** (a) Relative amounts of DCE isomers (1,1-DCE, *cis*-1,2-DCE, and *trans*-1,2-DCE) at 40% PCE conversion, for Pd-on-Au NPs of various Pd surface coverages (dashed lines mark the selectivity values averaged over the 10–150 sc% range. (b) Comparison of DCE isomer distributions for Pd-on-Au NPs (averaged over the 10–150 sc% range), Pd NPs, and $Pd/Al_2O_3$ at 40% PCE conversion.

1,1-DCE (1519 $L/g_{Pd}$/min) under similar experimental conditions [47].

The same adsorption explanation extended somewhat to Pd(1 1 1) surfaces. *trans*-1,2-DCE, 1,1-DCE and *cis*-1,2-DCE had calculated adsorption energies of −0.75, −0.69, and −0.65 eV, respectively, on Pd(1 1 1) [81], which superficially correlated with the solution-phase concentration trend of *trans*-1,2-DCE < 1,1-DCE < *cis*-1,2-DCE. The large difference in *trans*-1,2-DCE concentration between the Pd NP and $Pd/Al_2O_3$ cases was not accounted for, due in part to Pd(1 1 1) being a poor structural model of nanoparticulate Pd.

### 3.5. Reaction mechanism

PCE HDC led to the formation and subsequent degradation of TCE, DCE isomers, and VC, similar to TCE HDC. For the TCE HDC reaction, DCE's and ethene formed in small amounts and then degraded to non-detectable levels; ethane was the dominant product, with butane/butenes as the minor side-products (<3%) at the end of the reaction [46,47,79,82]. The concentration-time profiles (Fig. 3) of the partially dechlorinated products, $C_2$ compounds, and $C_4$ compounds suggested the following general PCE HDC reaction pathway: after dissolving into water, PCE dechlorinates and hydrogenates one Cl group at a time, eventually forming ethene which hydrogenates into ethane (Scheme 1). Carbon-coupling of ethene surface species led to butene/butane formation. These $C_4$ products were detected with Pd-on-Au NPs and Pd NPs in previous studies on TCE HDC [46,79,82]. Observed through surface enhanced Raman spectroscopy was $C_4$ species chemisorbed on a Pd-on-Au surface, which formed during 1,1-DCE HDC reaction [83]. Lowry and Reinhard reported the formation of $C_4$–$C_6$ products (1-butene, *n*-butane, *cis*-2-butene, *trans*-2-butene, and 2-hexene) with $Pd/Al_2O_3$ during TCE HDC [84].

A modified Langmuir-Hinshelwood kinetic model was developed by assuming that the gas-to-liquid mass transfer and the reversible chemisorption of surface species for the various compounds to be in quasi-equilibrium (Scheme S1). This modeling approach implies that all surface reactions are rate-limiting and does not require a reaction step to be identified as rate-limiting [85–87].

A set of differential equations (Eqs. (1)–(8)) implicitly describing concentration-time profiles for the ten possible chemical species are as follows:

$$\frac{d[\mathrm{PCE}]}{dt} = -\beta \times k_{\mathrm{PCE}}[\mathrm{PCE}] \tag{1}$$

$$\frac{d[\mathrm{TCE}]}{dt} = \beta \times \left( k_{\mathrm{PCE}} \frac{K_{\mathrm{PCE}}}{K_{\mathrm{TCE}}}[\mathrm{PCE}] - \sum_i k_{\mathrm{TCE}_i}[\mathrm{TCE}] \right) \tag{2}$$

$$\frac{d[\mathrm{DCE}_i]}{dt} = \beta \times \left( k_{\mathrm{TCE}_i} \frac{K_{\mathrm{TCE}}}{K_{\mathrm{DCE}_i}}[\mathrm{TCE}] - k_{\mathrm{DCE}_i}[\mathrm{DCE}]_i \right) \quad (i = 1,1-\mathrm{DCE},\ \mathrm{trans}-1,2-\mathrm{DCE},\ \mathrm{cis}-1,2-\mathrm{DCE}) \tag{3}$$

$$\frac{d[\mathrm{VC}]}{dt} = \beta \times \left( \sum_i k_{\mathrm{DCE}_i} \frac{K_{\mathrm{DCE}_i}}{K_{\mathrm{VC}}}[\mathrm{DCE}]_i - k_{\mathrm{VC}}[\mathrm{VC}] \right) \tag{4}$$

$$\frac{d[\mathrm{ethene}]}{dt} = \beta \times \frac{K_{\mathrm{VC}}}{K_{\mathrm{ethene}}} k_{\mathrm{VC}}[\mathrm{VC}] - \beta^2 \times k_{\mathrm{ethene1}}[\mathrm{ethene}] - 2\alpha[S]_{\mathrm{total}} K_{\mathrm{ethene}} k_{\mathrm{ethene2}}[\mathrm{ethene}]^2 \tag{5}$$

$$\frac{d[\mathrm{butene}]}{dt} = \alpha[S]_{\mathrm{total}} \times \frac{K_{\mathrm{ethene}}^2}{K_{\mathrm{butene}}} k_{\mathrm{ethene2}}[\mathrm{ethene}]^2 - \beta \times k_{\mathrm{butene}}[\mathrm{butene}] \tag{6}$$

$$\frac{d[\mathrm{butane}]}{dt} = \beta \times \frac{K_{\mathrm{butene}}}{K_{\mathrm{butane}}} k_{\mathrm{butene}}[\mathrm{butene}] \tag{7}$$

$$\frac{d[\mathrm{ethane}]}{dt} = \beta \times \frac{K_{\mathrm{VC}}}{K_{\mathrm{ethane}}} k_{\mathrm{VC}}[\mathrm{VC}] \tag{8}$$

where $\alpha = 1/1 + \sqrt{K_{H_2}[H_2]_0}$, $\beta = \sqrt{K_{H_2}[H_2]_0}\alpha[S]_{\mathrm{total}}$

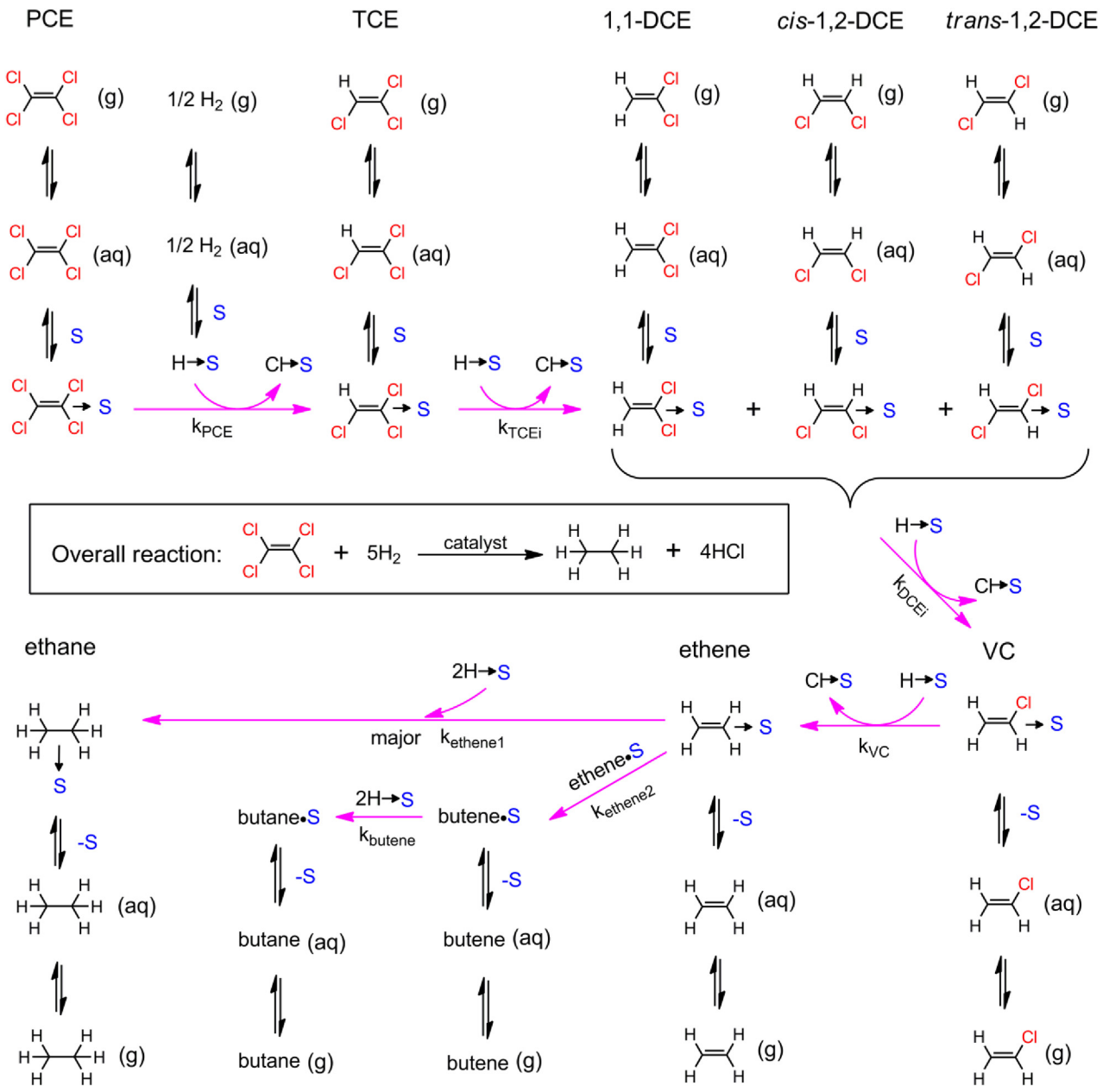


**Scheme 1.** Proposed reaction pathway of heterogeneously catalyzed PCE HDC, which includes gas-to-liquid transfer as an elementary step. "*S*" represents catalytic active sites. "*k*" under the arrows represents corresponding surface reaction rate constant.

The numerical solutions to the differential equations were least-squares fit to the concentration-time profiles using *Matlab* (solid lines of Fig. 3; *Matlab* code provided in Supplementary Information). The coefficient of determination $R^2$ was >0.96, indicating a very good fit between the data and fitted curves. Species with zero or trace concentrations, such as ethene, butanes, and butane, were not included, to minimize fitting error. The fitted parameters for each catalyst type are listed in Table S3. The relative standard error for most fitted parameters was <10% (except for those associated with VC, which was ~35%).

**Table 1**
Selected fitted kinetic parameters using modified Langmuir-Hinshelwood kinetics model.

| Species | Fitted kinetic parameters | 60 sc% Pd-on-Au NPs | Pd NPs | $Pd/Al_2O_3$ |
|---|---|---|---|---|
| PCE | $\beta k_{PCE}$ | 0.082 ± 0.006 | 0.015 ± 0.001 | 0.093 ± 0.007 |
| TCE | $\frac{k_{PCE}}{k_{TCE}}$ | 0.29 ± 0.02 | 0.0034 ± 0.0003 | 0.019 ± 0.002 |
| | $\beta \sum_i k_{TCE_i}$ | 0.51 ± 0.03 | 0.075 ± 0.007 | 1.5 ± 0.12 |
| DCE's | $\beta \sum_i k_{DCE_i}$ | 1.5 ± 0.14 | 0.14 ± 0.01 | 1.5 ± 0.14 |
| VC | $\beta k_{VC}$ | 0.90 ± 0.3 | 0.11 ± 0.04 | Not fitted |

Table 1 lists selected fitted parameters for which conclusions can be drawn. The relation, $\sum_i k_{DCE_i}$ (the sum of reaction rate constants of all DCE's degrading to VC) $\geq \sum_i k_{TCE_i}$ (the sum of reaction rate constants of TCE degradation to all DCE isomers) $> k_{PCE}$ (the rate constant of PCE degradation to TCE), held for all three catalyst types. The concentration profiles of Fig. 3 thus show the first step in the PCE HDC surface reaction pathway (the reductive replacement of Cl with H group) to be the slowest, using any of the catalysts tested. With the first Cl group removed from PCE, it becomes progressively faster to remove the subsequent Cl groups. This trend is consistent with other reports that compare the relative reactivities of chlorinated ethenes [44,47]. Not following this trend is the rate constant of VC degradation to ethene ($k_{VC}$), which was smaller than $\sum_i k_{DCE_i}$ for Pd-on-Au NPs and Pd NPs. This was probably due to the small amounts of VC detected and to concentration-time profiles of some chemical species (produced after VC degradation, Fig. 3) not being included when solving the differential equations. The concentration of VC for the $Pd/Al_2O_3$ case was too low to be detected, and not included in the fitting analysis.

## 4. Conclusions

PCE is a prevalent and hazardous groundwater contaminant similar to TCE, but its removal–especially through reduction catalysis–has not been studied as thoroughly. PCE and TCE are chemically related, and this study reveals significant differences in their catalytic conversion through HDC chemistry. Pd-on-Au NPs, Pd NPs, and $Pd/Al_2O_3$ successfully catalyze the HDC reaction of PCE in water, at room temperature, and at atmospheric pressure. The catalytic activity of Pd-on-Au NPs varies in a highly controllable manner with Pd surface coverage, with the most active composition having ~80 sc%. The volcano shape activity curve resembles the curve of TCE HDC except the latter has peak activity at 60–70 sc%, indicating the Pd-on-Au nanostructure can catalytically distinguish between the two closely related chlorinated ethene species. The appearance and sequential degradation of TCE, DCE isomers, VC, and ethene are evidence that the stepwise dechlorination of each chlorine group occurred for all catalysts tested. The relative amounts of detected DCE isomers differ among the 3 catalyst types, which is attributed to differences in adsorption affinities and reactivities of each isomer to the metal surface. Ethane is predominantly produced at the end of reaction, with the balance being *n*-butane and butenes. For PCE conversions > 85%, ethane selectivity is ~95%, ~88%, and 99% for Pd-on-Au NPs, Pd NPs, and $Pd/Al_2O_3$, respectively. A Langmuir-Hinshelwood kinetics model without determining a rate-limiting step *a priori* is developed, yielding concentration-time profiles that reasonably match experimental data and yielding relative rate constants that indicate PCE becomes increasingly reactive as it dechlorinates stepwise. This work demonstrates the much higher catalytic activity of Pd-on-Au NPs over Pd-only catalysts, showcasing a new approach in reduction catalysis to PCE contamination.

## Acknowledgments

This work is supported by NSF (CBET-1134535, EEC-0647452), the Welch Foundation (C-1676), and Sigma Xi Grants-in-Aid of Research program (G20111015157503). We acknowledge helpful discussions with Mr. R.J. Smith, Dr. S.-J. Li, Mr. J.C. Velazquez, and Ms. L.A. Pretzer.

## Appendix A. Supplementary data

Supplementary data associated with this article can be found, in the online version, at http://dx.doi.org/10.1016/j.apcatb.2013.04.032.

## References

[1] B. Linn, L. Appel, R. DeZeeuw, P. Doorn, J. Doyon, T. Evanson, J. Farrell, D. Hanson, R. Jurgens, J. So, C. Speigel, D. Switek, S. Yankey, State Coalition for Remediation of Drycleaners (2010).
[2] M.J. Moran, J.S. Zogorski, P.J. Squillace, Environmental Science and Technology 41 (2006) 74–81.
[3] U.S. EPA, IRIS Toxicological Review of Tetrachloroethylene (Perchloroethylene) (External Review Draft), EPA/635/R-08/011A, U.S. Environmental Protection Agency, Washington, DC, 2008.
[4] J.M. DeSimone, Science 297 (2002) 799–803.
[5] Siloxane D5 in Drycleaning Applications, EPA/744/F/03/0, U.S. Environmental Protection Agency, Washington, DC, 2005.
[6] P. Sinsheimer, R. Gottlieb, C. Farrar, Environmental Science and Technology 36 (2002) 1649–1655.
[7] J.F. Artiola, M.D. Ramírez, Chlorinated Solvent Contaminants in Arizona Aquifers, The University of Arizona, Tucson, AZ, 2006.
[8] Remediation of Chlorinated Solvent Contamination on Industrial and Airfield Sites, United States Air Force, Environmental Restoration Program, Brooks AFB, TX, 2000.
[9] National Primary Drinking Water Regulations, EPA/816/F/09/004, U.S. Environmental Protection Agency, Washington, DC, 2009.
[10] CERCLA Priority List of Hazardous Substances, Agency for Toxic Substances and Disease Registry, U.S. Department of Health and Human Services, Atlanta, GA, 2011.
[11] Groundwater quality and quantity in Europe, European Environment Agency, Copenhagen, 1999.
[12] White Paper: Perchloroethylene, European Chlorinated Solvent Association (ECSA), 2007.
[13] Water and health in Europe: a joint report from the European Environment Agency and the WHO Regional Office for Europe, European Environment Agency, WHO, 2002.
[14] J. He, Y. Li, S. Liu, H. Chen, Environment Science 26 (2005) 121–125.
[15] C.Y. Chan, J.H. Tang, Y.S. Li, L.Y. Chan, Atmospheric Environment 40 (2006) 7331–7345.
[16] C.S. Carr, J.B. Hughes, Environmental Science and Technology 32 (1998) 1817–1824.
[17] U.S. EPA, Toxicity and Exposure Assessment for Children's Health: Vinyl Chloride (VC), U.S. Environmental Protection Agency, Washington, DC, 2007.
[18] T.H. Wiedemeier, H.S. Rifai, C.J. Newell, J.T. Wilson, Natural Attenuation of Fuels and Chlorinated Solvents in the Subsurface, John Wiley & Sons, New York, 1999.
[19] C. Hofstee, J.H. Dane, W.E. Hill, Journal of Contaminant Hydrology 25 (1997) 235–247.
[20] O. Ayyildiz, R.W. Peters, Fresenius Environmental Bulletin 13 (2004) 1515–1517.
[21] A. Hirvonen, T. Tuhkanen, P. Kalliokoski, Water Science and Technology 33 (1996) 67–73.
[22] M.D. Nelson, B.L. Parker, T.A. Al, J.A. Cherry, D. Loomer, Environmental Science and Technology 35 (2001) 1266–1275.
[23] J. Costanza, G. Otano, J. Callaghan, K.D. Pennell, Environmental Science and Technology 44 (2010) 9445–9450.
[24] In situ Thermal Treatment of Chlorinated Solvents: Fundamentals and Field Applications, EPA/542/R/04/010, U.S. Environmental Protection Agency, Washington, DC, 2004.
[25] N. Cope, J.B. Hughes, Environmental Science and Technology 35 (2001) 2014–2021.
[26] C.M. Kao, S.C. Chen, J.Y. Wang, Y.L. Chen, S.Z. Lee, Water Research 37 (2003) 27–38.
[27] M. Schnarr, C. Truax, G. Farquhar, E. Hood, T. Gonullu, B. Stickney, Journal of Contaminant Hydrology 29 (1998) 205–224.
[28] J.A. Lackovic, N.P. Nikolaidis, G.M. Dobbs, Environmental Engineering Science 17 (2000) 29–39.
[29] A. Agrawal, P.G. Tratnyek, Environmental Science and Technology 30 (1996) 153–160.
[30] J. Farrell, M. Kason, N. Melitas, T. Li, Environmental Science and Technology 34 (2000) 514–521.
[31] G.D. Sayles, G.R. You, M.X. Wang, M.J. Kupferle, Environmental Science and Technology 31 (1997) 3448–3454.
[32] I.F. Cheng, R. Muftikian, Q. Fernando, N. Korte, Chemosphere 35 (1997) 2689–2695.
[33] S.F. O'Hannesin, R.W. Gillham, Ground Water 36 (1998) 164–170.
[34] R.T. Wilkin, R.W. Puls, G.W. Sewell, Ground Water 41 (2003) 493–503.
[35] A.D. Henderson, A.H. Demond, Environmental Engineering Science 24 (2007) 401–423.
[36] R.L. Johnson, R.B. Thoms, R.O. Johnson, T. Krug, Ground Water Monitoring and Remediation 28 (2008) 47–55.

[37] A. Taghavy, J. Costanza, K.D. Pennell, L.M. Abriola, Journal of Contaminant Hydrology 118 (2010) 128–142.
[38] H. Song, E.R. Carraway, Applied Catalysis B: Environmental 78 (2008) 53–60.
[39] S. Klimkova, M. Cernik, L. Lacinova, J. Nosek, Nano 3 (2008) 287–289.
[40] A. Amir, W. Lee, Chemical Engineering Journal 170 (2011) 492–497.
[41] S. Kovenklioglu, Z. Cao, N. Shah, R.J. Farrauto, E.N. Balko, AIChE Journal 38 (1992) 1003–1012.
[42] C.G. Schreier, M. Reinhard, Chemosphere 31 (1995) 3475–3487.
[43] G.V. Lowry, M. Reinhard, Environmental Science and Technology 33 (1999) 1905–1910.
[44] K. Mackenzie, H. Frenzel, F.-D. Kopinke, Applied Catalysis B: Environmental 63 (2006) 161–167.
[45] M.O. Nutt, J.B. Hughes, M.S. Wong, Environmental Science and Technology 39 (2005) 1346–1353.
[46] M.O. Nutt, K.N. Heck, P.J.J. Alvarez, M.S. Wong, Applied Catalysis B: Environmental 69 (2006) 115–125.
[47] M.S. Wong, P.J.J. Alvarez, Y.L. Fang, N. Akcin, M.O. Nutt, J.T. Miller, K.N. Heck, Journal of Chemical Technology and Biotechnology 84 (2009) 158–166.
[48] K.N. Heck, M.O. Nutt, P.J.J. Alvarez, M.S. Wong, Journal of Catalysis 267 (2009) 97–104.
[49] Y.L. Fang, K.N. Heck, P.J.J. Alvarez, M.S. Wong, ACS Catalysis 1 (2011) 128–138.
[50] Y.L. Fang, J.T. Miller, N. Guo, K.N. Heck, P.J.J. Alvarez, M.S. Wong, Catalysis Today 160 (2011) 96–102.
[51] M.G. Davie, H. Cheng, G.D. Hopkins, C.A. LeBron, M. Reinhard, Environmental Science and Technology 42 (2008) 8908–8915.
[52] E. Diaz, S. Ordonez, R.F. Bueres, E. Asedegbega-Nieto, H. Sastre, Applied Catalysis B: Environmental 99 (2010) 181–190.
[53] C.A. Gonzalez, C.M. de Correa, Industrial and Engineering Chemistry Research 49 (2010) 490–497.
[54] O. Orbay, S. Gao, B. Barbaris, E. Rupp, E. Saez, R.G. Arnold, E.A. Betterton, Applied Catalysis B: Environmental 79 (2008) 43–52.
[55] N.C. Concibido, T. Okuda, W. Nishijima, M. Okada, Reaction Kinetics and Catalysis Letters 89 (2006) 369–376.
[56] N.C. Concibido, T. Okuda, W. Nishijima, M. Okada, Reaction Kinetics and Catalysis Letters 90 (2007) 127–136.
[57] N.C. Concibido, T. Okuda, W. Nishijima, M. Okada, Applied Catalysis B: Environmental 71 (2007) 64–69.
[58] L.M. Kustov, E.D. Finashina, E.V. Shuvalova, O.P. Tkachenko, O.A. Kirichenko, Environment International 37 (2011) 1044–1052.
[59] H.-L. Lien, W.-x. Zhang, Colloids and Surfaces A: Physicochemical and Engineering Aspects 191 (2001) 97–105.
[60] R.-A. Doong, Y.-J. Lai, Water Research 39 (2005) 2309–2318.
[61] F. He, D. Zhao, C. Paul, Water Research 44 (2010) 2360–2370.
[62] J.W. Slot, H.J. Geuze, European Journal of Cell Biology 38 (1985) 87–93.
[63] ImageJ, v. 1.40. National Institutes of Health, 2008 (http://rsb.info.nih.gov/ij/).
[64] E. Wilhelm, R. Battino, R.J. Wilcock, Chemical Reviews 77 (1977) 219–262.
[65] D. Mackay, W.Y. Shiu, Journal of Physical and Chemical Reference Data 10 (1981) 1175–1199.
[66] J. Staudinger, P.V. Roberts, Environmental Science and Technology 26 (1996) 205–297.
[67] U.S. EPA, On-Line Tools for Site Assessment Calculation: Estimated Henry's Law Constants, U.S. Environmental Protection Agency, Washington, DC, 2009.
[68] T. Teranishi, M. Miyake, Chemistry of Materials 10 (1998) 594–600.
[69] J.M. Thomas, Pure and Applied Chemistry 60 (1988) 1517–1528.
[70] L. Lewis, Chemical Reviews 93 (1993) 2692–2730.
[71] P. Castellazzi, G. Groppi, P. Forzatti, A. Baylet, P. Marécot, D. Duprez, Catalysis Today 155 (2010) 18–26.
[72] D. Roth, P. Gélin, A. Kaddouri, E. Garbowski, M. Primet, E. Tena, Catalysis Today 112 (2006) 134–138.
[73] Soil Screening Guidance: Technical Background Document Table of Contents, EPA/540/R/95/128, U.S. Environmental Protection Agency, Washington, DC, 1996.
[74] C.J. Baddeley, R.M. Ormerod, A.W. Stephenson, R.M. Lambert, Journal of Physical Chemistry 99 (1995) 5146–5151.
[75] M. Baldauf, D.M. Kolb, Journal of Physical Chemistry 100 (1996) 11375–11381.
[76] D.I. Enache, J.K. Edwards, P. Landon, B. Solsona-Espriu, A.F. Carley, A.A. Herzing, M. Watanabe, C.J. Kiely, D.W. Knight, G.J. Hutchings, Science 311 (2006) 362–365.
[77] A. Roudgar, A. Groß, Physical Review B 67 (2003) 033409.
[78] A. Roudgar, A. Groß, Chemical Physics Letters 409 (2005) 157–162.
[79] L.A. Pretzer, H.J. Song, Y.-L. Fang, Z. Zhao, N. Guo, T. Wu, I. Arslan, J.T. Miller, M.S. Wong, Journal of Catalysis 298 (2013) 206–217.
[80] J. Dolfing, D.B. Janssen, Biodegradation 5 (1994) 21–28.
[81] J. Andersin, K. Honkala, Physical Chemistry Chemical Physics 13 (2011) 1386–1394.
[82] S. Li, Y.-L. Fang, C.D. Romanczuk, Z. Jin, T. Li, M.S. Wong, Applied Catalysis B: Environmental 125 (2012) 95–102.
[83] K.N. Heck, B.G. Janesko, G.E. Scuseria, N.J. Halas, M.S. Wong, Journal of the American Chemical Society 130 (2008) 16592–16600.
[84] G.V. Lowry, M. Reinhard, Environmental Science and Technology 35 (2001) 696–702.
[85] P. Chou, M.A. Vannice, Journal of Catalysis 107 (1987) 140–153.
[86] I. Hoek, T.A. Nijhuis, A.I. Stankiewicz, J.A. Moulijn, Applied Catalysis A: General 266 (2004) 109–116.
[87] P.A. Rautanen, J.R. Aittamaa, A.O.I. Krause, Chemical Engineering Science 56 (2001) 1247–1254.